Journal of Solid State Chemistry 183 (2010) 789–794

Contents lists available at ScienceDirect

Journal of Solid State Chemistry

journal homepage: www.elsevier.com/locate/jssc

Magnetic and thermodynamic properties of NdT_2Ge_2 (T=Pd, Ag) compounds

Ł. Gondek [a,*], B. Penc [b], D. Kaczorowski [c], S. Baran [b], A. Hoser [d], S. Gerischer [d], A. Szytuła [b]

[a] Faculty of Physics and Applied Computer Science, AGH University of Science and Technology, Mickiewicza 30, 30-059 Kraków, Poland
[b] M. Smoluchowski Institute of Physics, Jagiellonian University, Reymonta 4, 30-059 Kraków, Poland
[c] W. Trzebiatowski Institute of Low Temperature and Structural Research, Polish Academy of Sciences, PO Box 1410, 50-950 Wrocław, Poland
[d] BENSC, Helmholtz-Zentrum Berlin, Glienicker Str. 100, D-14 109 Berlin, Germany

ARTICLE INFO

Article history:
Received 7 December 2009
Received in revised form
27 January 2010
Accepted 30 January 2010
Available online 4 February 2010

Keywords:
Magnetically ordered material
Magnetic susceptibility
Specific heat
Electrical resistivity
Neutron diffraction

ABSTRACT

Physical properties of $NdPd_2Ge_2$ and $NdAg_2Ge_2$, crystallizing with the tetragonal $ThCr_2Si_2$-type crystal structure, were investigated by means of magnetic, calorimetric, electrical transport as well as by neutron diffraction measurements. The specific heat studies and neutron diffraction measurements were performed down to 0.30 K and 0.47 K, respectively. Both compounds exhibit antiferromagnetic ordering below T_N equal to 1.5 K for $NdPd_2Ge_2$ and 1.8 K for $NdAg_2Ge_2$. Neutron diffraction data for the latter germanide indicate antiferromagnetic collinear structure described by the propagation vector $\boldsymbol{k}$=(0.5, 0, 0.5). The Nd magnetic moments equal to 2.24(5) μ_B at 0.47 K are aligned along the a-axis and have the + − sequence within the crystal unit cell. For $NdPd_2Ge_2$ only very small Bragg peaks of magnetic origin were observed in the neutron diffraction patterns measured below T_N, thus hampering determination of the magnetic structure. Both compounds exhibit metallic-like electrical conduction. From the specific heat data the crystal electric field (CEF) levels schemes were determined. Difference between the overall CEF splitting in the two compounds is correlated with their structural parameters.

1. Introduction

Ternary rare-earth intermetallic compounds RT_2X_2 (R=rare earth, T=d-electron transition metal and X=Si or Ge) have been intensively studied for their intriguing physical behaviour [1,2]. Most of these phases crystallize in the body-centred tetragonal structure of the $ThCr_2Si_2$-type (space group $I4/mmm$) [3], in which the R, T and X atoms occupy 2a, 4d and 4e sites, respectively.

Among RT_2X_2 phases definitely least known are the germanides containing light rare earths (R=Ce, Pr, Nd, Sm) and 4d transition elements (T=Pd, Ag). The reported X-ray diffraction data indicate that these compounds form the $ThCr_2Si_2$-type crystal structure [4,5]. The RAg_2Ge_2 (R=Ce, Nd, Sm) compounds are antiferromagnets with the Nèel temperatures equal to 4.6 K for R=Ce [6], 2 K for R=Nd [7,8] and 10 K for R=Sm [8]. For $PrAg_2Ge_2$ the magnetic susceptibility showed a broad maximum at 12 K [7,8], while the neutron diffraction data did not reveal Bragg peaks that might hint at any kind of long-range magnetic ordering [7]. Magnetometric measurements performed for single-crystalline $NdAg_2Ge_2$ sample revealed the ordering temperature of 2 K and metamagnetic like transitions corroborating the antiferromagnetic ordering [9]. In turn, the magnetic studies of the RPd_2Ge_2 (R=Ce, Pr, Nd) established an antiferromagnetic order below 5.1 K for R=Ce [10,12], 5.0 K for R=Pr and 1.3 K for R=Nd [12]. Neutron diffraction measurements indicated the magnetic structures describable by the propagation vector $\boldsymbol{k}$=(0.285, 0, 0.9) for $CeAg_2Ge_2$ [13], $\boldsymbol{k}$=(0.5, 0.5, 0.16) for $CePd_2Ge_2$ [11], $\boldsymbol{k}$=(0, 0, 1/3) for $PrPd_2Ge_2$ [12]. For $NdAg_2Ge_2$ some diffraction peaks of small intensity were observed in the neutron diffraction pattern measured at 1.5 K, which were indexed with the propagation vector $\boldsymbol{k}$=(0.5, 0, 0.5) [7]. For $NdPd_2Ge_2$ no neutron diffraction data were reported so far.

In order to clarify the magnetic properties of the two latter compounds, we performed new studies by means of magnetic susceptibility, magnetization, electrical resistivity, specific heat and neutron diffraction measurements.

2. Experimental

Polycrystalline samples of $NdPd_2Ge_2$, $LaAg_2Ge_2$ and $NdAg_2Ge_2$ were synthesized by arc melting of high-purity elements (Nd: 3 N; Pd and Ag: 4 N; Ge: 5 N) in a titanium gettered argon atmosphere. Subsequently, the samples were annealed in an evacuated quartz tubes at 1073 K for one week. Quality of the products was examined by X-ray powder diffraction at room temperature on the Philips PW-3710 X'PERT diffractometer using Cu$K\alpha$ radiation. The obtained data were analyzed using the Rietveld-type refinement program FullProf [14]. All the reflections were indexed in the tetragonal $ThCr_2Si_2$-type structure. The determined values

* Corresponding author.
E-mail address: lgondek@agh.edu.pl (Ł. Gondek).

0022-4596/$ - see front matter © 2010 Elsevier Inc. All rights reserved.
doi:10.1016/j.jssc.2010.01.031

Table 1
Lattice parameters a and c, their ratio a/c, unit cell volume V, positional parameter z of the Ge-atom in $NdPd_2Ge_2$ and $NdAg_2Ge_2$, as derived from the X-ray data collected at room temperature and the neutron diffraction data at 4 K. R_{Bragg} and R_{prof} are the reliability factors of the structure refinements.

Compound	$NdPd_2Ge_2$		$NdAg_2Ge_2$	
T(K)	300	4.0	300	4.0
a(Å)	4.3040(5)	4.294(1)	4.2623(3)	4.254(5)
c(Å)	10.0366(17)	10.080(4)	11.0145(8)	11.010(9)
a/c	0.4288(2)	0.3860(2)	0.3870(1)	0.3864(7)
V(Å^3)	185.92(8)	185.86(16)	200.10(3)	199.24(63)
z	0.3783(5)	0.3781(8)	0.3895(5)	0.3893(5)
R_{Bragg}(%)	5.0	6.7	7.1	5.9
R_{prof}(%)	8.1	7.4	8.4	8.4

of the structural parameters of $NdPd_2Ge_2$ and $NdAg_2Ge_2$ are listed in Table 1. They are in good agreement with the data reported earlier.

Magnetic measurements were performed in the 1.72–400 K temperature range and in external magnetic fields up to 5 T using the Quantum Design MPMS-5 SQUID magnetometer. The electrical resistivity was measured over the temperature interval of 4.2–300 K employing the standard dc four-probe technique. Specific heat studies were carried our in the 0.3–300 K temperature range by relaxation method employing a Quantum Design PPMS platform.

Neutron diffraction patterns were recorded at the E6 diffractometer installed at the BER II reactor at the BENSC—Helmholtz Zentrum Berlin. The incident neutron wavelength was 2.452 Å. The powdered samples were enclosed in a cylindrical copper container with a diameter of 8 mm. For better thermal contact a small amount of deuterated methanol was dropped into container. The data were collected at several different temperatures between 0.47 and 4.0 K using an ILL-type cryostat with a ^{3}He insert. The data were analysed using above mentioned FullProf software.

3. Results

3.1. Magnetic behaviour

The magnetic properties of $NdPd_2Ge_2$ are presented in Fig. 1. In the entire studied temperature range the inverse magnetic susceptibility exhibits a linear-in-T behaviour. Fitting the Curie–Weiss law yields the paramagnetic Curie temperature $\theta_p = -10.1(3)$ K and the effective magnetic moment $\mu_{eff} = 3.78(2)\,\mu_B$. These values are similar to those reported in Ref. [12]. The value of μ_{eff} is slightly larger that the free Nd^{3+} ion value ($3.62\,\mu_B$). As seen from the upper inset to Fig. 1, the compound remains paramagnetic down to 1.72 K. The isothermal magnetization measured at this terminal temperature corroborates the paramagnetic state.

The magnetic data for $NdAg_2Ge_2$ were reported in our previous work (see Fig. 1 in Ref. [7]). In the temperature dependence of the magnetic susceptibility a faint maximum near 2 K was observed. Above this temperature the reciprocal magnetic susceptibility obeyed the Curie–Weiss law with $\theta_p = -10.0$ K and $\mu_{eff} = 3.72(5)\,\mu_B$. The negative of sign θ_p is in line with the antiferromagnetic character of the magnetic ordering in the compound. Further evidence for the antiferromagnetic ground state came from a quasi-linear behaviour of the isothermal magnetization taken at 1.72 K as a function of magnetic field. The magnetic moment measured in a field of 5 T was equal to $1.3\,\mu_B$, i.e. it was much smaller than the free ion value for Nd^{3+} ion ($3.27\,\mu_B$).

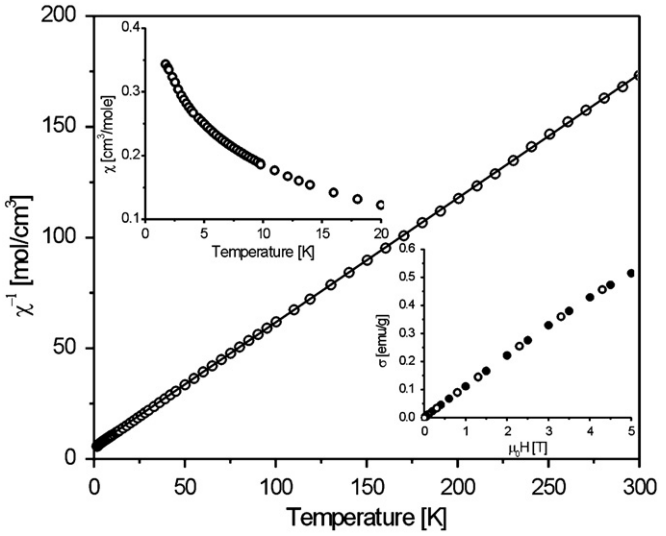

Fig. 1. Temperature dependence of the reciprocal magnetic susceptibility of $NdPd_2Ge_2$. The solid line represents the fit of the Curie–Weiss formula (see the text for details). The upper inset shows the magnetic susceptibility at low temperatures. The lower inset presents the isothermal magnetization curve taken at 1.7 K. The filled and open circles refer to the data collected with increasing and decreasing the magnetic field strength, respectively.

3.2. Specific heat studies

The results of heat capacity measurements of $NdPd_2Ge_2$ are presented in Fig. 2. Some anomalous behaviour of $C_p(T)$ can be noticed below 25 K, which likely arises due to magnetic contribution to the specific heat. At higher temperatures, $C_p(T)$ is dominated by the phonon contribution that was assumed to be similar to that in the nonmagnetic $LaAg_2Ge_2$ reference sample. The entire specific heat of the latter compound can be approximated using a formula

$$C_{ph+el} = 9R\frac{1}{1-\alpha T}\left(\frac{T}{\Theta_D}\right)^3\int_0^{\Theta_D/T}\frac{x^4e^x}{(e^x-1)^2}\,dx + R\frac{1}{1-\alpha T}\sum_i\frac{(\Theta_{Ei}/T)^2e^{\Theta_{Ei}/T}}{(e^{\Theta_{Ei}/T}-1)^2} + \gamma T \quad (1)$$

where R stands for the gas constant, Θ_D is the Debye temperature, Θ_{Ei} are the Einstein temperatures, γ represents the electronic specific heat coefficient and α is the anharmonic coefficient. It is assumed that in the studied compounds there are 3 acoustic modes (described by the first term of Eq. (1)) and 12 optical modes (described by the second term of Eq. (1)). For simplicity the optical modes were grouped into triple degenerated branches. Fitting Eq. (1) to the experimental data of $LaAg_2Ge_2$ following set of parameters was obtained: $\Theta_D = 165(1)$ K; $\Theta_{E1} = 80.5(6)$ K; $\Theta_{E2} = 154(1)$ K; $\Theta_{E3} = 247(2)$ K; $\Theta_{E4} = 394(4)$ K; $\alpha = 2.21(2)\times10^{-4}$ K^{-1} and $\gamma = 5.2(1)$ mJ/mole K^2. The so-obtained characteristic temperatures were rescaled with respect to different molar masses of the investigated compounds and let us to derive the nonmagnetic contribution to the specific heat of $NdPd_2Ge_2$ in the form of the function presented in Fig. 2a by the solid line. The rescaled Debye temperature yields $\Theta_D = 164.5$ K.

The magnetic specific heat, estimated by subtracting the phononic and electronic contributions from the measured $C_p(T)$ data, is shown in Fig. 2b. The broad anomaly centred at about 15 K originates from lifting degeneracy of the ground $^4I_{9/2}$ multiplet of

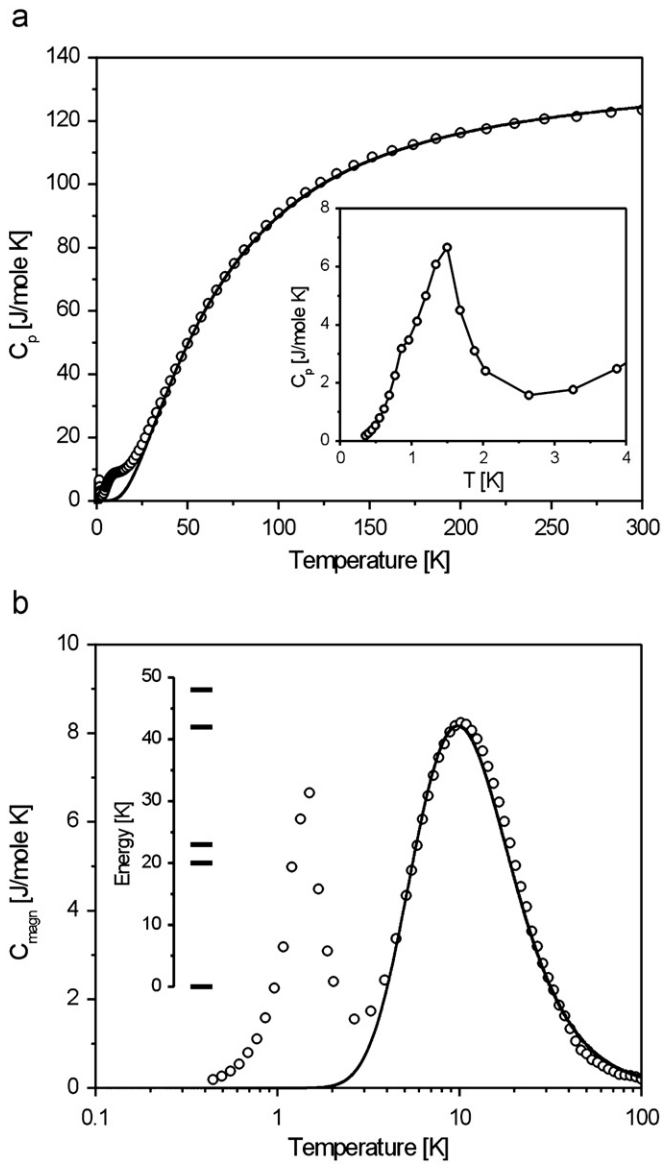

Fig. 2. (a) Temperature dependence of the specific heat of $NdPd_2Ge_2$. The solid curve is the calculated nonmagnetic contribution (for details see the text). The inset presents the specific heat at low temperatures. (b) The magnetic contribution to the specific heat of $NdPd_2Ge_2$ (open symbols) with the Schottky fit discussed in the text. The inset shows the derived crystal field levels scheme.

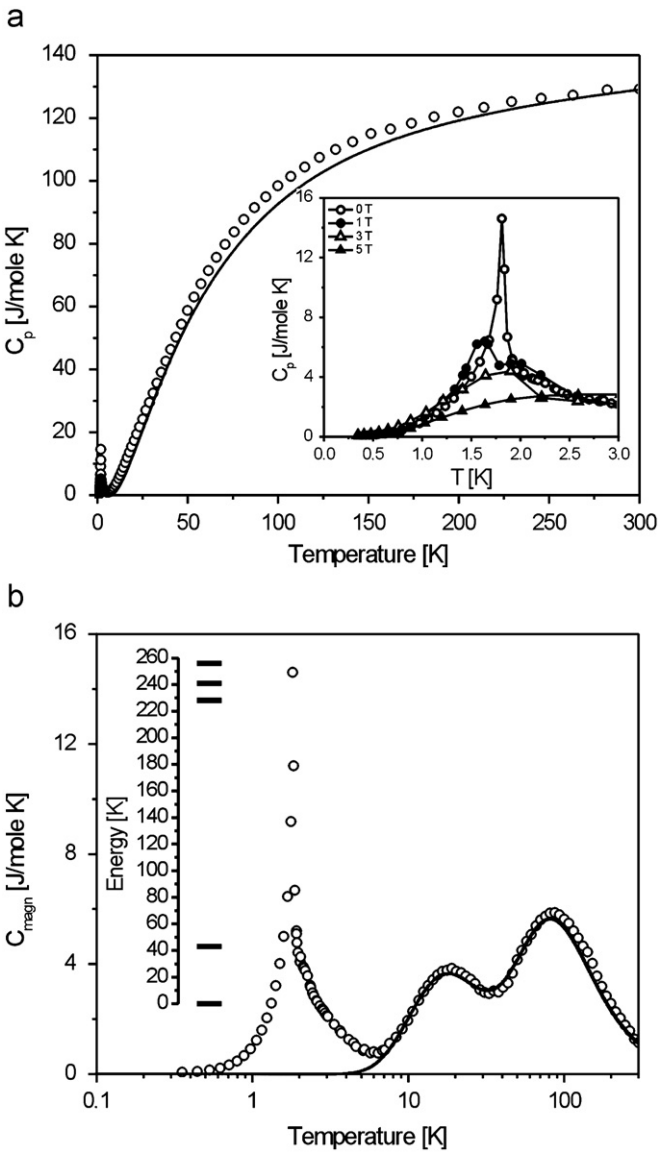

Fig. 3. (a) Temperature dependence of the specific heat of $NdAg_2Ge_2$. The solid curve is the calculated nonmagnetic contribution (for details see the text). The inset presents the specific heat at low temperatures and under presence of magnetic field. (b) The magnetic contribution to the specific heat of $NdAg_2Ge_2$ (open symbols) with the Schottky fit discussed in the text. The inset shows the derived crystal field levels scheme.

the Nd^{3+} ions in the tetragonal crystal electric field (CEF) potential. It can be described in terms of the Schottky contribution for the CEF levels splitting scheme presented in the inset to Fig. 2b. It consists of five doublets splited by 48 K, with the first excited state located about 20 K above the ground state. The latter doublet undergoes splitting in the ordered state, that arises at 1.50(5) K, and the splitting manifests itself as a sharp anomaly in $C_p(T)$. As it is best apparent from the inset to Fig. 2a, another very weak anomaly in the specific heat data seem to occur at 0.85(5) K. This latter feature may arise from hypothetical change in the magnetic structure of $NdPd_2Ge_2$, yet this conjecture requires verification in further experiments.

In the case of $NdAg_2Ge_2$, the measured specific heat data (see Fig. 3a) were analyzed in a similar way as described above, with the rescaled Debye temperature Θ_D=163.9 K. This procedure let us to calculate the purely magnetic contribution to the specific heat, presented in Fig. 3b. Quite surprisingly, the Schottky effect in this compound was found to be distinctly different from that in $NdPd_2Ge_2$, namely two broad specific heat maxima located at about 20 and 100 K were evidenced. Analysis of the CEF splitting yielded the levels scheme sketched in the inset to Fig. 3b. Here, the total splitting of the $^4I_{9/2}$ multiplet is as large as 256 K, with the first excited doublet placed more than 40 K above the ground level.

The low-temperature specific heat of $NdAg_2Ge_2$ is dominated by a sharp anomaly at 1.80(5) K (see Fig. 3a). This feature can be unambiguously attributed to the ordering of the Nd magnetic moments. Moreover, above T_N an extended tail in $C_p(T)$ is seen. Upon applying external magnetic field of 1 T, the main peak shifts towards lower temperatures, hence signalling antiferromagnetic character of the ordered state (see inset to Fig. 3a), whereas the tail evolves into a fairly well maximum near 2 K. In stronger fields, a single broad hump is observed in $C_p(T)$, which shifts to higher temperatures with increasing field, as might be expected for antiferromagnets above their metamagnetic phase transition.

3.3. Electrical resistivity measurements

Fig. 4 displays the temperature variations of the electrical resistivities of $NdPd_2Ge_2$ and $NdAg_2Ge_2$. Both compounds exhibit metallic-like behaviour with the room temperature resistivity of 76 and 116 μΩ cm, respectively, which drops to 4 and 11 μΩ cm, respectively, at liquid helium temperature. For none of them anomalies related to the magnetic ordering were observed because of the experimental range limited to 4.2 K.

In the paramagnetic region, the resistivity data of $NdPd_2Ge_2$ can be analysed in terms of Bloch–Grüneisen–Mott (BGM) formula

$$\rho(T) = (\rho_0 + \rho_\infty) + 4AT\left(\frac{T}{\theta_R}\right)^4 \int_0^{\theta_R/T} \frac{x^5\,dx}{(e^x-1)(1-e^{-x})} - KT^3 \qquad (2)$$

where the first term stands for the scattering of conduction electrons on static defects in the crystal lattice (residual resistivity ρ_0) as well as on disordered magnetic moments (the spin-disordered resistivity ρ_∞), the second term stands for the electron–phonon scattering (θ_R is a characteristic temperature of the order of the Debye temperature) and the last one originates from interband *s–d* scattering (so-called Mott term).

As seen in Fig. 4a, a satisfactory description of the experimental $\rho(T)$ curve of $NdPd_2Ge_2$ by the BGM function was obtained above about 50 K. In this temperature region the crystal field effect is negligible (i.e. ρ_∞=const), as established from the above discussed specific heat data. The least-squares fit parameters were found as follows: $\rho_0+\rho_\infty = 10.3(1)$ μΩ cm, $A = 0.26(1)$ μΩ cm/K; $\theta_R = 239.5(4)$ K and $K = 2.7(1)\times 10^{-7}$ μΩ cm/K^3. Below 50 K, the resistivity of $NdPd_2Ge_2$ is progressively smaller and smaller than that calculated from Eq. (2), which arises due to gradual depopulation of excited crystal field levels with decreasing temperature.

In the case of $NdAg_2Ge_2$ the CEF splitting is as large as nearly 260 K, thus there is no extended temperature interval, where the BGM approach might be valid. Therefore, no attempt was made to analyze the ρ(T) data of this compound in terms of Eq. (2).

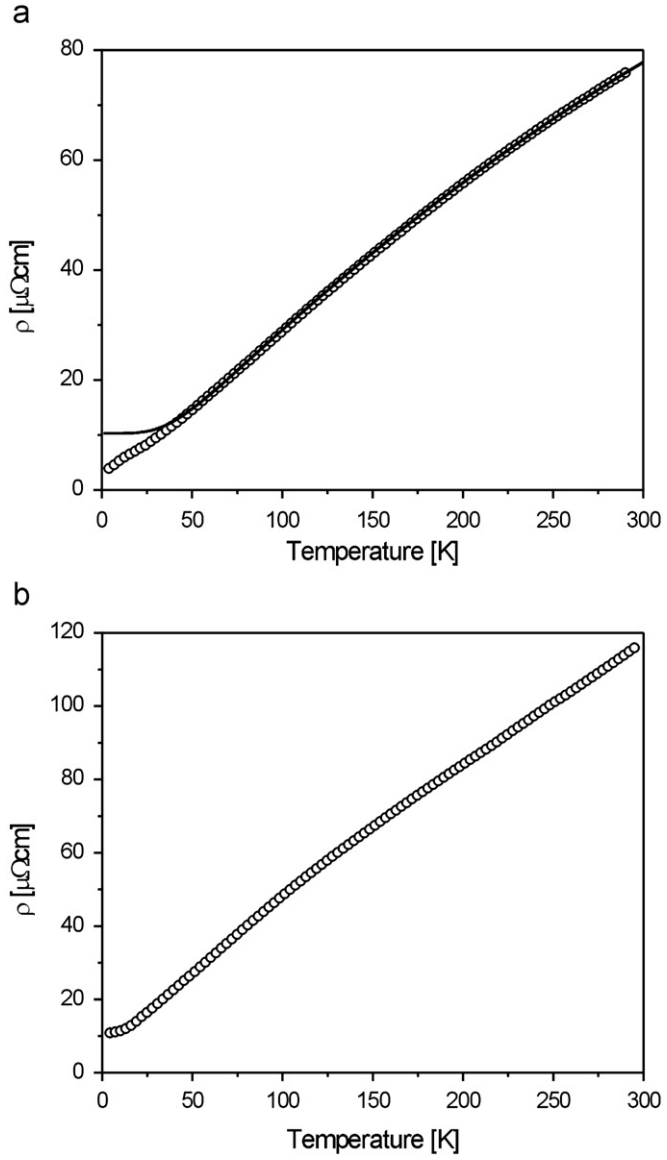

Fig. 4. Temperature variations of the electrical resistivity of $NdPd_2Ge_2$ (a) and $NdAg_2Ge_2$ (b). The solid line in panel (a) represents the fit of the Bloch–Grüneisen–Mott formula, described in the text.

3.4. Neutron diffraction

The neutron diffraction patterns recorded at 4 K for $NdPd_2Ge_2$ and $NdAg_2Ge_2$ are shown in the upper panels of Figs. 5 and 6, respectively. These data confirm for both compounds the tetragonal structure of the $ThCr_2Si_2$-type (space group *I4/mmm*). In the unit cell, the Nd atoms occupy the 2(a) sites: (0, 0, 0),

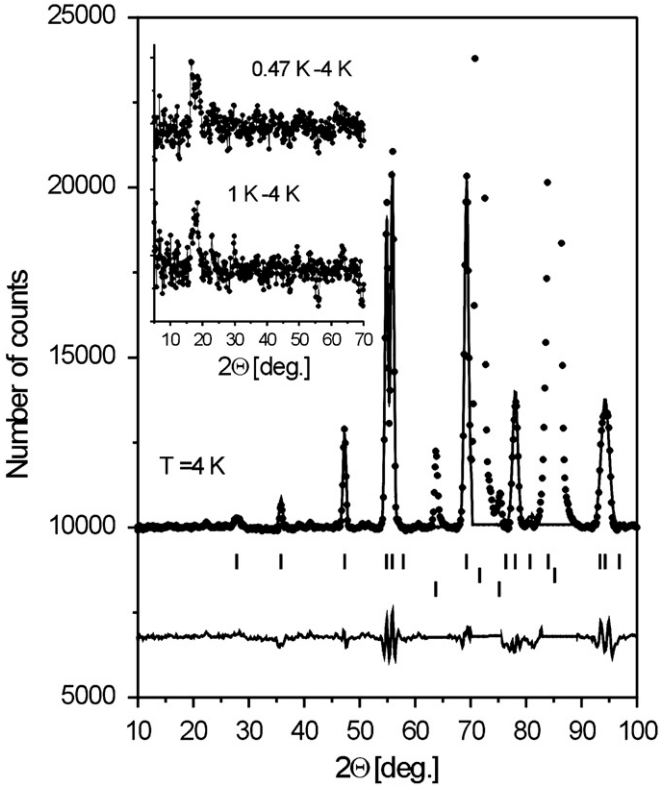

Fig. 5. Neutron diffraction pattern of $NdPd_2Ge_2$ collected at 4 K. The circles represent the experimental points and the solid line through the data is the calculated profile for the crystal structure model as described in the text. The vertical bars indicate the Bragg peaks of nuclear origin. Some regions were not taken into account as they contain peaks originating from copper sample container (note the second row of Bragg's reflections) and aluminium parts of cryostat (note the third row of Bragg's reflections). The difference between the observed and calculated intensities is shown by the solid line at the bottom of the panel. The insets present the difference patterns 0.47–4 K and 1–4 K (see the text for details).

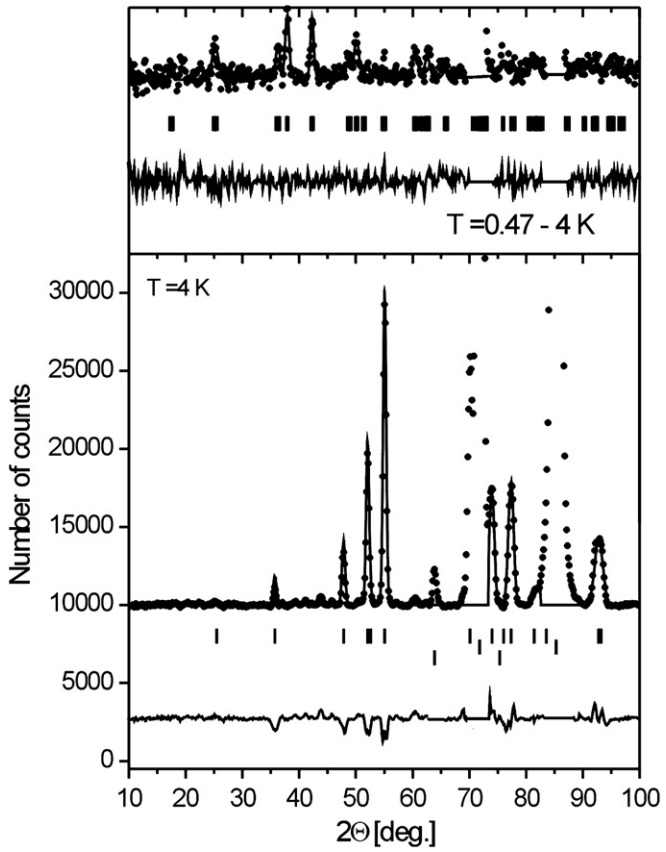

Fig. 6. Neutron diffraction pattern of $NdAg_2Ge_2$ collected at 4 K (lower panel) and the difference pattern 0.47–4 K (upper panel). The circles represent the experimental points, and the solid curves are the calculated profiles for the model crystal and magnetic structures described in the text. The vertical bars indicate the Bragg peaks of nuclear and magnetic origin, in the lower panel and the upper panel, respectively. The differences between the observed and calculated intensities are presented at the bottom of each panel. Some regions were not taken into account as they contain peaks originating from copper sample container (note the second row of Bragg's reflections) and aluminium parts of cryostat (note the third row of Bragg's reflections).

the Ag or Pd atoms are located at the 4d sites: (0, 1/2, 1/4) and (1/2, 0, 1/4), while the Ge atoms occupy the 4e sites: (0, 0, z) and (0, 0, $-z$) (the atoms are located at these and the symmetry equivalent positions). The refined values of the lattice parameters as well as those of the positional parameter z, which correspond to the minimum of the reliability factor, are listed in Table 1.

In order to extract the magnetic contributions to the neutron patterns collected at 0.47 and 1 K the difference patterns 0.47–4.0 and 1–4.0 K for $NdPd_2Ge_2$ and 0.47–4.0 K for $NdAg_2Ge_2$ were calculated. These patterns, together with corresponding paramagnetic diffraction patterns, are shown in Figs. 5 and 6, respectively. In the case of $NdPd_2G_2$, two peaks at 2θ equal 16.3 and 18.1 deg can be noticed in the 0.47–4.0 K difference pattern, while only one broad feature at 2θ=17.8 deg can be resolved in the1–4.0 K pattern. From the data it is not possible to determine the magnetic structure of this compound. On the other hand, the difference pattern of $NdAg_2Ge_2$ contains several additional peaks of the magnetic origin. Their analysis yielded a collinear antiferromagnetic structure described by the propagation vector $\boldsymbol{k}$=(0.5, 0, 0.5). At 0.47 K, the magnetic moments carried by the Nd atoms located at the (0, 0, 0) and (1/2, 1/2, 1/2) positions are equal to 2.24(5) μ_B. The moments are aligned along the a-axis and have a $+-$ sequence within the crystallographic unit cell. This magnetic structure type agrees with the previous prediction for $NdAg_2Ge_2$ [7].

4. Concluding remarks

The ternary NdT_2Ge_2 (T=Pd, Ag) compounds crystallize with the tetragonal $ThCr_2Si_2$-type crystal structure and exhibit antiferromagnetic ordering below 1.5 K for $NdPd_2Ge_2$ and 1.8 K for $NdAg_2Ge_2$, as derived from the specific heat and neutron diffraction data. In the latter compound a spin-reorientation may take place at 0.85 K. For both ternaries the Nèel temperature is smaller than those reported for the isostructural RPd_2Ge_2 and RAg_2Ge_2 (R=Ce, Pr, Sm) phases. The observed reduction indicates that the magnetic behaviour in these germanides is likely not solely governed by RKKY-type interactions but also influenced by some other mechanisms. Namely, the failure of de Gennes scaling suggest that crystal field effects must be taken into account. On the other hand, hybridisation of the Nd4f states with transition metal 4d states may be another factor influencing the magnetic exchange. Similar irregular dependencies of the Nèel temperature along the rare earth element has been observed in a few other RT_2X_2 series [1,2].

The Nd magnetic moment in $NdAg_2Ge_2$ being equal to 2.24(5) μ_B is much smaller than the free ion Nd^{3+} value (3.27 μ_B), and should be attributed to the crystal field ground doublet state. Strong evidence for the CEF effect in both compounds studies comes also from the bulk magnetic, electrical transport and specific heat data. The CEF Hamiltonian appropriate for the tetragonal symmetry can be written as

$$H_{CEF} = B_2^0O_2^0 + B_4^0O_4^0 + B_4^4O_4^4 + B_6^0O_6^0 + B_6^4O_6^4$$

where B_n^m and O_n^m are the CEF parameters and the Stevens operators, respectively. It is well known (for discussion see e.g. Ref. [1]) that for the RT_2X_2 compounds, the second-order parameter usually determines the direction of the magnetic moment, namely for $B_2^0 < 0$ the c-axis is the easy axis of magnetization, whereas for $B_2^0 > 0$ the easy magnetization axis lies within the basal plane. In the case of Nd-based ternaries $NdCu_2Si_2$ [15], $NdCu_2Ge_2$ [16] and $NdFe_2Si_2$ [17], the CEF parameter B_2^0 is negative. Indeed it is consistent with the observed direction of the moment along the c-axis. Similarly, negative sign of B_2^0 may be deduced for $NdAg_2Ge_2$, where the Nd magnetic moment is also parallel to the c-axis.

The total crystal field splitting in $NdAg_2Ge_2$ is much larger than that in $NdPd_2Ge_2$. Table 2 lists the magnitudes of the CEF splitting ΔE in a few NdT_2Ge_2 compounds in relation to the ratio a/c of the tetragonal unit cell parameters. Apparently, the value of ΔE decreases with increasing a/c, with exception for $NdAu_2Ge_2$ [18]. This feature originates in systematic changes in the interatomic distances between the Nd atom and its d-electron ligands in the coordination polyhedron of the Nd atom, which is somewhat disturbed for the latter phase. Similar correlation between the values of ΔE and the a/c ratio has been reported for hexagonal $NdAl_pGa_{2-p}$ system [19].

Table 2
Overall CEF splitting ΔE, a/c ratio and Nd–T ligand distances (in Å) for NdT_2Ge_2 compounds.

Compound	ΔE(K)	a/c	d_{Nd-T}	Ref.
$NdAg_2Ge_2$	256	0.387	3.4820	This work
$NdCu_2Ge_2$	154	0.407	3.2802	[15]
$NdPd_2Ge_2$	48	0.429	3.3056	This work
$NdAu_2Ge_2$	43	0.416	3.4060	[17]

Acknowledgments

This research project has been partially supported by the European Commission under the 6th Framework Programme through the Key Action: Strengthening the European Research Area, Research Infrastructures. Contract no: RII3-CT-2003-505925 (NMI3).

References

[1] A. Szytuła, J. Leciejewicz, in: K.A. Gschneidner Jr., L. Eyring (Eds.), Handbook on the Physics and Chemistry of Rare Earths, vol. 12, North Holland, Amsterdam, 1989, p. 133.
[2] D. Gignoux, D. Schmitt, in: K.H.J. Buschow (Ed.), Handbook of Magnetic Materials, vol. 10, Elsevier Science B.V., Amsterdam, 1997, p. 239.
[3] Z. Ban, M. Sikirica, Acta Crystallogr. 18 (1965) 594.
[4] P. Salamakha, P. Zaplatynsky, O. Sologub, O. Bodak, J. Alloys Compd. 239 (1996) 94.
[5] D. Rossi, R. Marazza, R. Ferro, J. Less-Common. Met. 66 (1979) 17.
[6] A. Thamizhavel, R. Kulkarni, S.D. Dhar, Phys. Rev. B 75 (2007) 144426.
[7] A. Szytuła, M. Bałanda, D. Kaczorowski, S. Baran, Ł. Gondek, J. Hernandez-Velasco, B. Penc, N. Stüsser, E. Wawrzyńska, Intermetallics 14 (2006) 315.
[8] Devang A. Jashi, R. Nagalakshmi, R. Kulkarni, S.X. Dar, A. Thamizhavel, Physica B 404 (2009) 2988.
[9] D.A. Joshi, R. Nagalakshimi, R. Kulkarni, S.K. Dhar, A. Thamizhavel, Physica B 404 (2009) 2988.
[10] R. Feyerherm, B. Becker, M.F. Collins, J. Medoch, G.J. Nieuwenhuys, S. Ramakrishnen, Physica B 241–243 (1998) 643.
[11] B. Fåk, E. Ressouche, G. Knebel, J. Flouquet, P. Lejay, Solid State Commun. 115 (2000) 407.
[12] R. Welter, K. Halioh, J. Phys. Chem. Solids 67 (2006) 862.
[13] A. Loidl, K. Knorr, G. Knopp, A. Krimmel, R. Caspary, A. Böhm, G. Sparn, C. Geibl, F. Steglich, A.P. Murani, Phys. Rev. B 46 (1992) 9341.
[14] J. Rodriguez-Carvajal, Physica B 192 (1993) 55.
[15] E.A. Goremychkin, A.Yu. Myzuchka, R. Osborn, JETP 83 (1996) 738.
[16] T. Shigeoka, K. Hivata, H. Mitamura, Y. Umatoko, T. Goto, Physica B 346–347 (2004) 117.
[17] P. Swoboda, J. Vejpravova, F. Honda, E. Santava, O. Schneeweiss, T. Komatsubara, Physica B 328 (2003) 139.
[18] A. Szytuła, D. Kaczorowski, L. Gondek, A. Arulraj, S. Baran, B. Penc, J. Magn. Magn. Mater. 321 (2009) 3402.
[19] A. Furrer, O.E. Martin, J. Phys. C: Solid State Phys. 19 (1986) 3863.